ELSEVIER

Polymer 42 (2001) 1969–1980

polymer

www.elsevier.nl/locate/polymer

Isothermal crystallization of polyethylene monitored by in situ NMR and analyzed within the "Avrami" model framework

P.E. Kristiansen[a,*], E.W. Hansen[b], B. Pedersen[a]

[a]*Department of Chemistry, University of Oslo, P.O. Box 1033, Blindern, 0315 Oslo, Norway*
[b]*SINTEF Applied Chemistry, P.O. Box 124, Blindern, 0314 Oslo, Norway*

Received 3 November 1999; received in revised form 11 May 2000; accepted 9 June 2000

Abstract

The shape of the solid-state proton NMR Free Induction Decay (FID) of a molten polyethylene (PE) sample has been examined as a function of time during isothermal crystallization in situ. The crystallization rate as a function of crystallization temperature is derived and the results discussed within a thermodynamic framework. A slight increase in molecular correlation times (in the microsecond range) with crystallization time was revealed for both the crystalline and intermediate phases. In particular, the molecular mobility within the intermediate phase is found to be approximately four times faster than in the crystalline phase. During isothermal crystallization the more mobile molecular phase is claimed to be composed of two "sub-phases", an amorphous phase and a molten phase. The latter "sub-phase", which represents 100% of the polymer at the start of the crystallization (completely molten sample), transforms completely to crystalline, amorphous and intermediate phases during the crystallization process. The actual temperature region of super-cooling, which can be probed by the present NMR technique, covers approximately 10 K and is discussed in the text.

Keywords: Avrami model; Spin–lattice relaxation; Polyethylene

1. Introduction

It is well known that crystallization and processing of polymers will affect their morphology [1,2]. In particular, much effort has been exercised in understanding the effect of crystallization on morphology [2–6], as this may affect the physical properties of the polymer [7]. Having once established that certain polymeric materials are capable of crystallization, fundamental studies related to the mode and kinetics of crystallization have been reported [2,8–10]. Numerous reports in the literature show that NMR spectroscopy is a powerful tool in characterizing polymer morphology [3–6,11,12]. For instance, NMR spectroscopy has given evidence that at least three phases are involved during crystallization of polyethylene (PE) and that the degree of crystallinity is dependent on the preparation of the polymer [3,4,11,12].

We have recently presented an in situ NMR technique, which enables monitoring of phase changes of PE during melting [13] and crystallization [14]. Due to an increasing rate of crystallization with increasing super-cooling, this NMR technique will only be appropriate within a restricted temperature region of super-cooling. For instance, if the PE crystallizes too rapidly, reliable crystallization rates cannot be extracted. Temperature regulation control, heat transfer, NMR relaxation times and crystallization rates are parameters which will determine the actual temperature range at which isothermal crystallization can be monitored by the present NMR technique. Spin–lattice relaxation times can be found in the literature [15–17]. However, the actual region of super-cooling, which enables reliable crystallization rates to be determined by the present NMR technique, can at present only be established experimentally.

Some NMR results reported by Kristiansen et al. [14] suggest that the spin–spin relaxation time (T_2) of the amorphous phase of PE as a function of crystallization time can be described by an Avrami type of function. In the present work, we will look more into this matter by applying the solid-state proton NMR Free Induction Decay (FID)-analysis technique [13,14,18] to monitor the phase changes taking place during isothermal crystallization of PE, *at different temperatures*. Also, information regarding molecular dynamics within the crystalline and the intermediate phases during isothermal crystallization will be reported.

The current work is part of an activity aiming at evaluating the capability of the solid-state proton NMR FID technique to monitor phase changes and molecular dynamics during crystallization and melting of PE, in situ.

* Corresponding author.

0032-3861/01/$ - see front matter
PII: S0032-3861(00)00443-2

2. Experimental

2.1. Material

The two PE samples used in this work were received from Borealis AS and contained 4–5 butyl branches per 1000 main chain carbons (sample A) and 4–5 butyl branches per 10 000 main chain carbons (sample B). The corresponding molecular weights were $M_W = 66\,000$ (sample A) and $M_W = 22\,000$ (sample B), respectively. The type and degree of branching were determined by high-resolution ^{13}C NMR[13]. Both samples were single site polymerized polymers. The samples were initially kept at 420 K for 30 min within the NMR magnet to ensure complete melting. Samples A and B were then cooled to 400 and 408 K for 10 min, respectively, before the temperature was set to the actual temperature at which isothermal crystallization was monitored. The time of the last temperature setting was defined as the onset of crystallization (zero time). Isothermal crystallization were monitored in situ at 391, 392, 393, 393.5, 394, 394.5 and 395 K for sample A and 399, 400, 401 and 402 K for sample B.

2.2. NMR

All NMR measurements were performed on a Bruker DMX 200 AVANCE instrument operating at 200 MHz proton resonance frequency. A high-power ^1H NMR probe capable of producing 90° radio frequency (r.f.) pulses of approximately 1.5 μs was used. Each point of the FID was sampled every 0.2 μs. To avoid pulse breakthrough, a receiver blanking time ("dead time") of 2 μs was applied. One scan was acquired in each experiment. Between 200 and 300 experiments were performed depending on crystallization temperature (the lowest number is for the lowest temperature investigated). The time delay between each experiment was initially set to 15 s, which is more than 5 times the longer spin–lattice relaxation time T_1, to ensure quantitative sampling of the FID. This time delay was changed twice during the experiment to 75 and 625 s, respectively (only one increase was done for the crystallization investigated at 392 K). The actual phase parameters were adjusted manually to give a pure absorption spectrum in order to ensure that only the real part of the FID was sampled.

Each FID was sampled for 4.4 ms, resulting in 22 K of data points. Before transferring the data to a PC for post processing, the data matrix was reduced in size by selecting the first 200 data points (from 2 to 42 μs) and the next 500 data points (42 μs–4.4 ms, i.e. every 44 point) of the residual part of the FID. This particular selection of data points was favored by visual inspection of all sampled FIDs, simultaneously. This data reduction, or filtering, was performed simply to speed up the subsequent calculations when using an Excel spread sheet and the program "solver".

The temperature within the probe was calibrated by a NMR thermometer of ethylene glycol and controlled by a Bruker B-VT2000 unit. The actual temperature was estimated to be stable and accurate to within ±0.5 K.

3. Theoretical outline

Due to r.f.-pulse breakthrough, it is necessary to introduce a receiver dead time during acquisition. This approach is known to affect both the shape and the intensity of the resulting frequency spectrum (Fourier-Transform of the FID) since the FID is truncated at early sampling times. If the shape of the FID components, representing the different phases (crystalline, intermediate and amorphous), were a priori known, a linear combination of these components could be fitted directly to the observed (truncated) FID. Unfortunately, these theoretical FID shapes are not a priori known. However, in Section 3.1 we will present some analytical functions [13,14,18], which are known to give reasonable representations of the different FID components.

3.1. The crystalline phase

Pake [19] derived an analytical expression for the NMR frequency spectrum of coupled spin 1/2 nuclei. Due to the inherent NMR dilemma related to r.f.-pulse breakthrough [20], this theoretical function can — in many cases — not be fitted directly to the frequency spectrum. Rather, one may derive the inverse Fourier Transform of the Pake function, which will represent the observed signal intensity in the time domain (FID). Look and co-workers [21] presented an analytical solution to this enigma, which has been used recently with success [13,14,18].

$$P(t) = \sqrt{\frac{\pi}{6}} \exp\left[-\frac{1}{2}\beta^2 t^2 \right] \left\{ \frac{\cos \alpha t}{\sqrt{\alpha t}} C\left[\sqrt{\frac{6\alpha t}{\pi}} \right] + \frac{\sin \alpha t}{\sqrt{\alpha t}} S\left[\sqrt{\frac{6\alpha t}{\pi}} \right] \right\} \quad (1)$$

where $P(t)$ defines the normalized time dependent FID. The α parameter is related to the distance, R_{H-H}, between the two nearest neighbor protons of the methylene group, and β represents the width of the Gaussian broadening function, which takes account of dipole–dipole interactions between protons on different methylene groups. $C[x]$ and $S[x]$ are the so-called Fresnel functions, which are defined as simple integral equations [22].

3.2. Non-crystalline phases

In contrast to the crystalline phase of PE, the amorphous and intermediate phases are evidenced by an increased fluctuation in the molecular mobility, which is expected to modify the shape of the NMR spectrum. A theoretical expression for the FID of these phases has been presented by Brereton et al. [23], and successfully applied in a recent

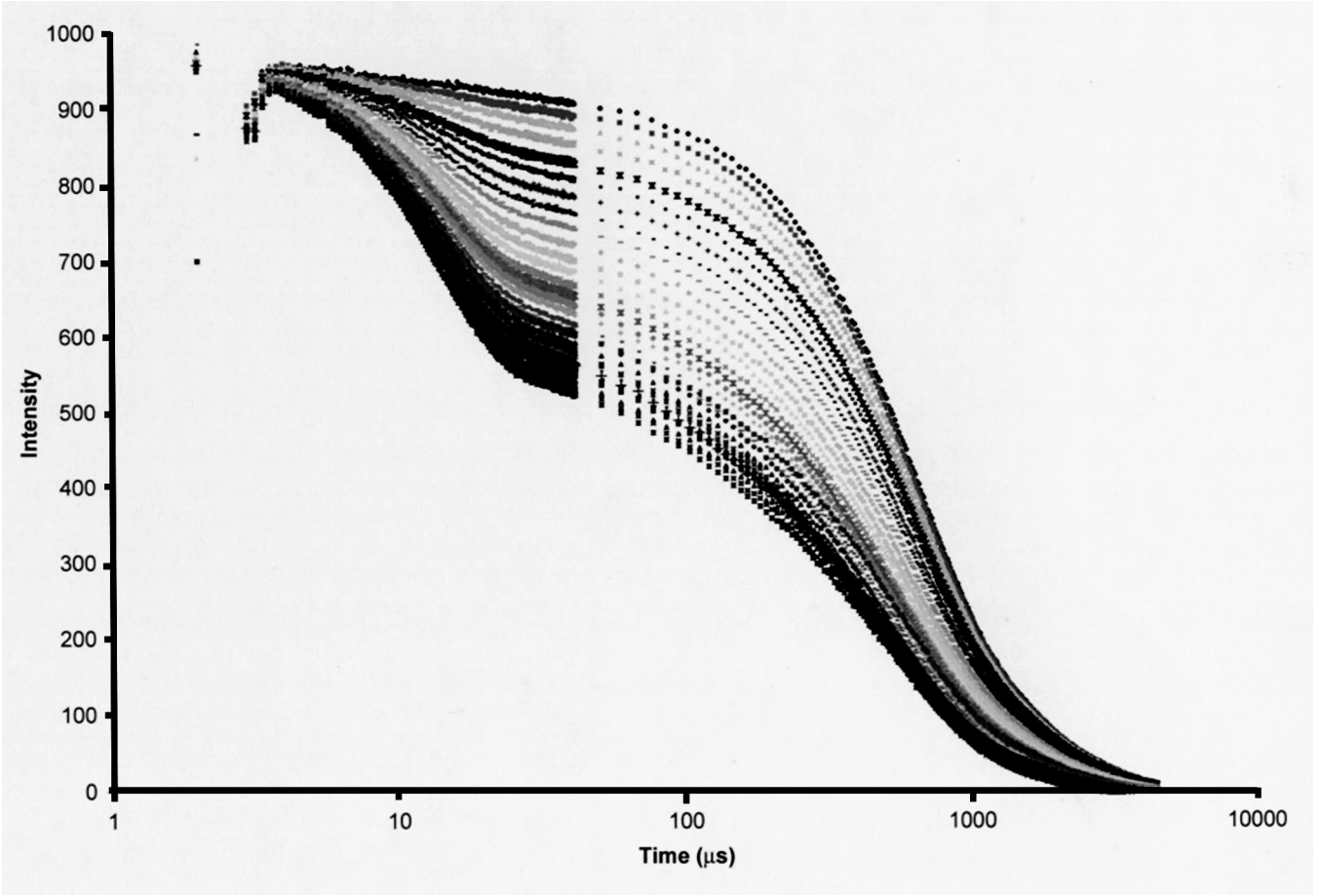

Fig. 1. Observed ^{1}H FIDs of PE during isothermal crystallization at 392 K. The FIDs are acquired at times (min): 4, 4.5, 5, 5,5, 6.5, 7, 7.5, 8, 8.5, 9, 9.5, 10, 10.5, 11, 11.5, 12.5, 13.5, 14, 16.5, 19, 21.5, 24, 29, 34, 39, 75.5, 146.5, 249 and 443.75 (from top to bottom).

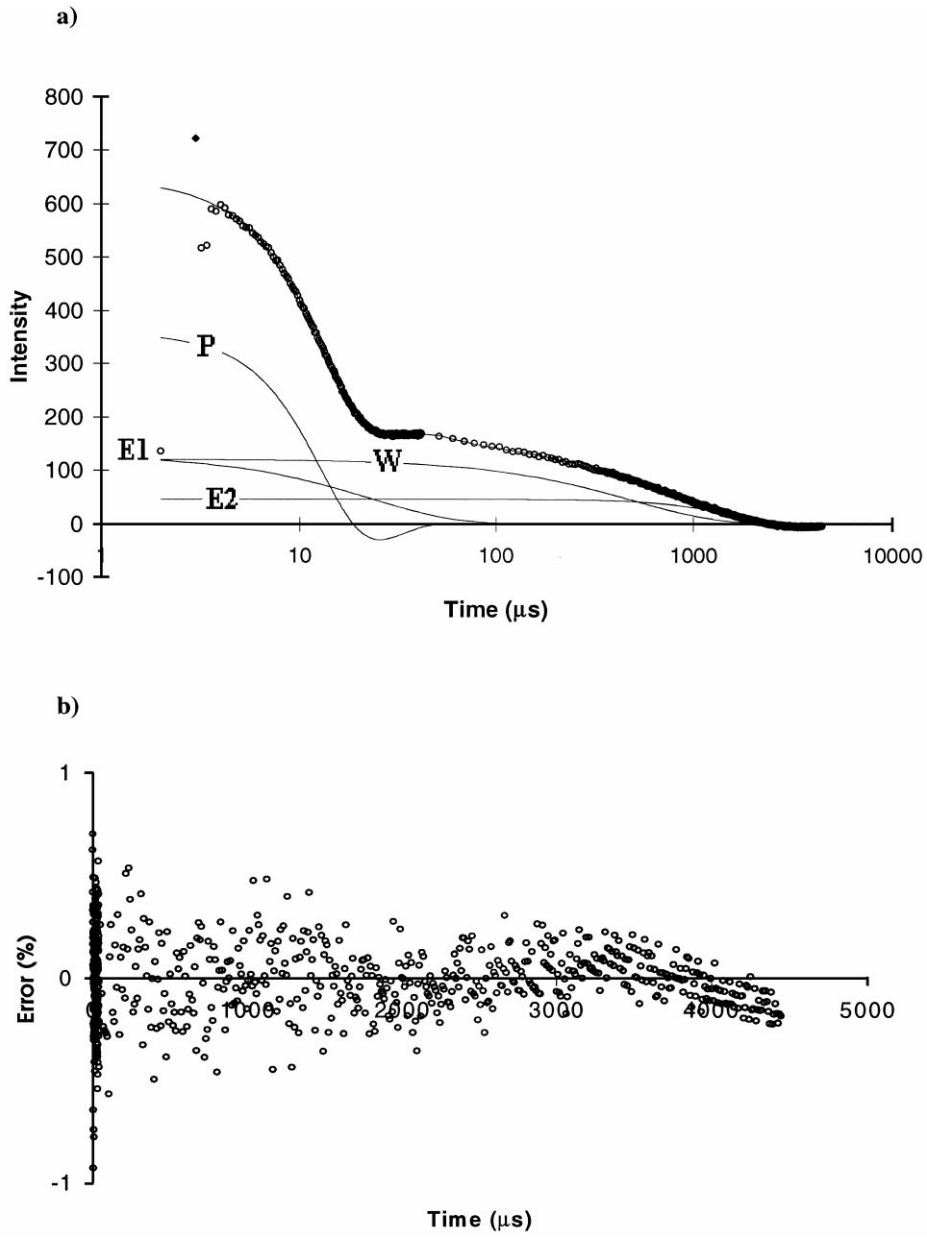

Fig. 2. (a) The four fitted FID-components (PWEE-model) sample B at the end of the isothermal crystallization at 399 K; ◆ experimental, the thin line through the points is the fit. P, E_1, W and E_2 curves are the decaying curves from left to right, or fast and slow. (b) Residual of the fit.

investigation on PE at room temperature [18]. Dadayli et al. [24] and Kristiansen et al. [13,14] have shown empirically that the FID of the amorphous phase can be well approximated by the sum of an Exponential function and a Weibullian function:

$$W(t) = \exp\left[-\left(\frac{t}{T_2}\right)^n\right] \tag{2}$$

where the normalized Weibullian function $W(t)$ ranges between a pure Exponential ($n = 1$) and a pure Gaussian ($n = 2$) function.

3.3. The Avrami equation

To describe the relative change in phase composition (amorphous, intermediate and crystalline phases) of PE during the crystallization process a slightly modified version of the Avrami equation [25,26] has been adopted:

$$\Theta_X(t) = \Theta_{X\infty} - (\Theta_{X\infty} - \Theta_{X0}) \exp(-[kt]^\beta) \tag{3a}$$

where $\Theta_X(t)$ defines the fraction of phase X formed after time t. The parameters k and β represent the rate constant and the Avrami exponent, respectively. The former parameter depends on nucleation rate and growth rate, while

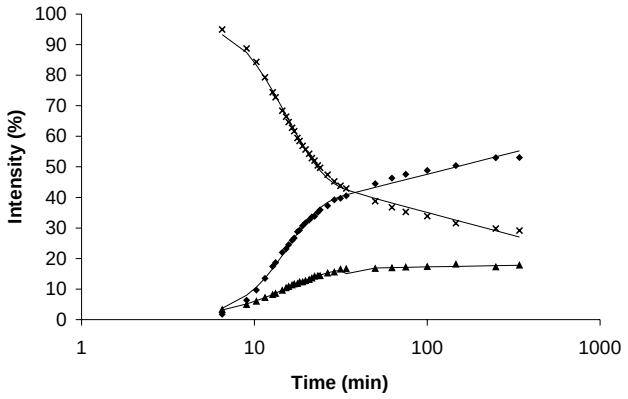

Fig. 3. Relative intensities of the four fitted FID-components (PWEE-model) sampled at: 400 K ◆ P; ▲ E_1; × $E_2 + W$. The solid line is the fit to Eq. (3).

the latter parameter depends on the nature of nucleation, the rate of polymer transport to the growing crystal, and the growth geometry [27]. In the original work by Avrami, the parameter $\Theta_{X\infty}$ represents the fraction of crystalline material formed at infinite time and was set equal to 1. In general, however, $\Theta_{X\infty}$ of the crystalline phase may be less than 1 [27]. Θ_{X0} represents the amount of phase X at time $t = 0$. For any phase X, which is initially zero ($\theta_{X0} = 0$), Eq. (3a) simplifies to the Avrami equation.

Other researchers in the field have suggests that the crystallization process cannot be simply described by a single-stage process [10,28]. Rather, a two-stage process has to be invoked. Such a two-stage process can be described mathematically by a two-step function composed of two time functions in series. If the fraction undergoing secondary crystallization is represented by the function $L(t)$, the following generalized equation, $\Psi(t)$, will predict the mass fraction of phase X at any time t during the crystallization process:

$$\psi_X(t) = \Theta_X(t) + L_X(t) \tag{3b}$$

From the observed time evolution of crystallization at longer times the following empirical function, $L_X(t)$, was chosen [14].

$$L_X(t) = \begin{cases} 0 & t < t_d \\ A_X + B_X \ln(t) & t \geq t_d \end{cases} \tag{3c}$$

where A_X and B_X are constants. A logarithmic time evolution of the secondary crystallization process represents an empirical model first proposed and applied by Kovacs [29] using density measurements. The time parameter t_d defines the onset of the secondary crystallization regime.

Recently a new model for the crystallization has been suggested in the literature [49–51], suggesting a spinodal decomposition caused by density fluctuations due to phase separation between all *trans* and, *trans–gauche* conformations. In this theory, it is assumed that the interchain ordering and the intrachain ordering happens at different times, while it in the classical theory is assumed that they happen at the same time. The kinetics of the crystallization process is, however, similar to the Avrami process [49], the Avrami function was therefore used in the analysis of the phase changes.

4. Results and discussion

4.1. Isothermal crystallization of PE-FID analysis

Fig. 1 shows a series of FID signals of molten PE (sample A) as a function of time after being placed within the magnet at 392 K. The FID changes shape with time due to onset of crystallization. The formation of a crystalline/intermediate phase is recognized by the relative increase of a fast decaying FID component ($t < 20$ μs) with increasing reaction time. The significantly large residuals observed at times less than 4 μs are caused by r.f.-pulse breakthrough (Fig. 1). These initial data points were excluded from the model fit in order to obtain more reliable and quantitative results. A more extensive discussion on this topic can be found in recent published work [13,18].

The theoretical FID applied in this work is simply denoted "PWEE" where the capital letters represent the Pake function (P; Eq. (1)), the Weibullian function (W; Eq. (2) with $1 \leq n \leq 2$), and the two Exponential functions (E; Eq. (2) with $n = 1$). This model equation was fitted to the observed FID by a non-linear least-squares technique and is illustrated in Fig. 2. Due to the small amount of crystalline phase formed at the early stage of the crystallization process, the two parameters α and β of the Pake function and the rate constant $1/T_{2,E_1}$ of the fast decaying Exponential function, could not be reliably determined for sample A. In recent published work [13], the parameters α and T_{2,E_1} were shown to vary only slightly with temperature within the temperature region 360–393 K. Hence, within the narrow temperature region investigated in this work (391–395 K) the parameters α and T_{2,E_1} were considered to be constant and equal to $\alpha = 1.15 \times 10^5$ s^{-1} and $T_{2,E_1} =$ 26 μs [13] at all times during the crystallization process. For sample B, the higher crystallinity allows these parameters to be determined by model fitting, the results of this will be discussed later. It must be emphasized, however, that the implicit assumption that the Pake function uniquely defines the crystalline phase of PE is somewhat ambiguous [13,14].

The exponential function (E_1) having the shorter spin relaxation time was assigned to the intermediate phase [13,14]. It may well be, however, that a fraction of this FID-component is part of a more mobile fraction of the crystalline phase, or an ordered mesophase which accidentally has the same T_2 as the intermediate phase (E_1).

Before ending this discussion, it is worth emphasizing that the crystallinity at room temperature determined by the present NMR technique is in agreement with the crystallinity derived by other methods [18]. A more detailed

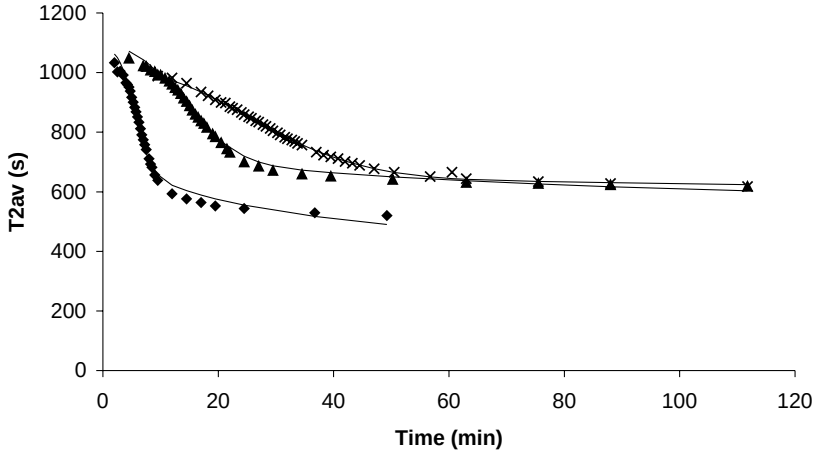

Fig. 4. $T_{2,av}$ vs. time: × 394.5 K; ▲ 393.5 K; ◆ 391 K sample A. The solid lines obtained from Eq. (5c). See text for further details.

investigation on this particular topic is in progress and will be reported.

The remaining two components (W and E_2) of the "PWEE"-model reveal significantly longer spin–spin relaxation times and are tentatively assigned to a phase composed of more mobile molecules and will be discussed in Section 4.2.

The relative distribution of the different FID-components (P, W, E_1 and E_2), as derived by model fitting, is a function of crystallization time and is illustrated in Fig. 3 (sample B at 400 K). The intensity distribution of the FID components as a function of crystallization time suggests that about 30% of the PE remains mobile (amorphous phase) after 2 h of isothermal crystallization. During the same time interval the amounts of crystalline and intermediate phases increase monotonically up to approximately 50 and 20%, respectively. The relative distribution of phases with time during isothermal crystallization at 394 K of sample A can be found in Ref. [14]. The intensity of the Pake-function (P) of this sample was approximately equal to or smaller than the intensity of the Exponential function (E_1) during the early stage of crystallization. However, at later crystallization times the intensity of the former became somewhat larger. The relative intensity of the fast decaying Exponential component (E_1) became approximately equal to the relative intensity of the intermediate phase of PE as observed by Kitamaru [12].

4.2. The mobile phase of PE

The Weibullian (W) and the Exponential (E) functions of the "PWEE" model are tentatively assigned to a more mobile (on a molecular level) phase in accordance with results reported by Bremner et al. [30], who used three Exponential functions to fit the FID of molten, low-molecular weight PE. The three FID-components were assigned to a non-network fraction, an amorphous entangled network fraction, and an ordered or high segmental-density fraction, in order of decreasing spin–spin relaxation times. Also, Brereton et al. [23] have suggested that the FID of melted polymers is not single exponential, as a result of entanglement.

In semi-crystalline PE, the existence of lamella structures may reduce the molecular mobility of the amorphous phase, implying that its T_2 may be less than T_2 of the completely molten sample.

In this work, the FID of molten PE prior to crystallization can be approximated by a sum of an Exponential function (E_2) and a Weibullian function (W). Moreover, two slow decaying FID components observed at any time during crystallization of the melted PE samples investigated in this work can also be approximated by a linear sum of these same two functions. Also, within the temperature range 391–395 K, a linear combination of these same two functions has been found to give a good representation of the amorphous phase FID of a non-melted PE [13].

Since only two FID components are needed to characterize the more mobile molecular phase, at any time during the crystallization process, an average spin–spin relaxation time $T_{2,av}$ is defined:

$$(W + E_2)\frac{1}{T_{2,\mathrm{av}}} = W\frac{1}{T_{2,W}} + E_2\frac{1}{T_{2,E_2}} \tag{5a}$$

where $T_{2,W}$ and T_{2,E_2} represent the spin–spin relaxation times of the two FID-components of intensity W and E_2, respectively.

Starting with a completely molten PE sample, we will assume that its average spin–spin relaxation time $T_{2,av}$ as a function of crystallization time can be expressed by:

$$\frac{1}{T_{2,\mathrm{av}}(t)} = f\frac{1}{T^{\mathrm{A}}_{2,\mathrm{av}}} + (1-f)\frac{1}{T^{\mathrm{M}}_{2,\mathrm{av}}} \tag{5b}$$

where $f = \mathrm{A}/(\mathrm{A} + \mathrm{M})$ defines the mole fraction at any time during crystallization of amorphous phase (A) within the mobile phase (A + M). Both A and M are time

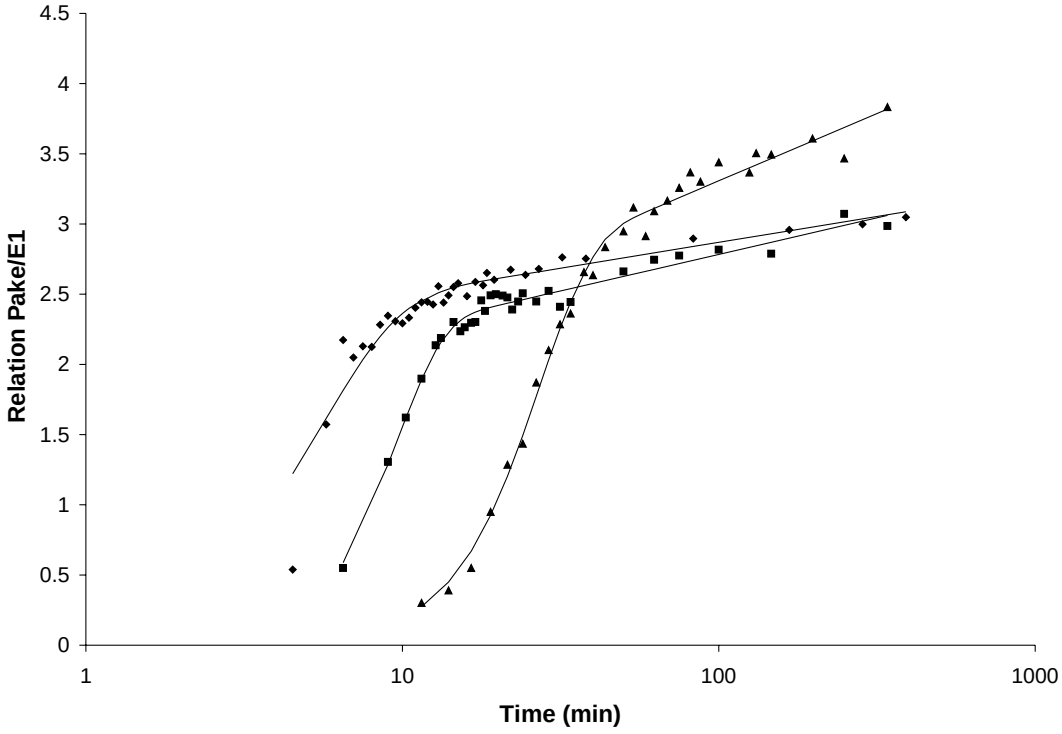

Fig. 5. The signal intensity ratio between the crystalline (Pake function) and the intermediate (Exponential function; E_1) phases vs. time: ◆ 399 K; ■ 400 K; ▲ 402 K sample B. The solid line is the fit to Eq. (3).

dependent functions, $T_{2,\mathrm{av}}^{\mathrm{X}}$ represents the average spin–spin relaxation time of phase X (= A and M) and is assumed to be time independent. Hence, at the start of crystallization the sample is completely molten ($M = M_0$), and transforms during crystallization into amorphous, crystalline and intermediate phases. In the intermediate time regime the mobile phase is composed of a mixture of the two phases A and M.

Assuming the intensity of molten (M) and amorphous phases (A) during the isothermal crystallization process to follow an Avrami type of function (Eq. (3a–c)), the following model equation can be derived (see Appendix A)

$$T_{2,\mathrm{av}}(t) = \frac{T_{2,\mathrm{A}}\, T_{2,\mathrm{M}}\{\theta_{\mathrm{A}\infty} - (\theta_{\mathrm{A}\infty} - 1)\exp(-[kt]^{\beta})\}}{\{\theta_{\mathrm{A}\infty} - \theta_{\mathrm{A}\infty}\exp(-[kt]^{\beta})\}\, T_{2,\mathrm{M}} + T_{2,\mathrm{A}}\exp(-[kt]^{\beta})} \tag{5c}$$

The average spin–spin relaxation times $T_{2,\mathrm{av}}$ of the mobile phase as a function of time during isothermal crystallization at 391, 393.5 and 394.5 K of sample A are shown in Fig. 4. Sample B showed similar time dependence. The solid curves are calculated from Eq. 5(c) by applying the k, β and t_{d} parameters derived from previous Avrami model fits to the intensity of the mobile phase as a function of temperature. Keeping in mind that the solid curves in Fig. 3 represent model fits to Eq. 5(c) with only two fitting parameters ($T_{2,\mathrm{av}}^{\mathrm{A}}$and $T_{2,\mathrm{av}}^{\mathrm{M}}$) they give a reasonable support to the assumption that the mobile phase (A + M) is composed of two characteristic and different phases, a molten phase (M) and an amorphous phase (A).

At longer crystallization times, i.e. after the primary crystallization is completed and the molten phase is no longer present, $T_{2,\mathrm{av}}$ still decreases slightly with time (approximated by a logarithmic time dependence). This reduction in $T_{2,\mathrm{av}}$ signifies a reduction of the molecular mobility of the amorphous phase and is tentatively explained by a lamella thickening, which affects the molecular mobility of the amorphous phase. This assumption is indirectly supported by noting that: (1) the signal intensity of the intermediate phase is approximately constant; and (2) the signal intensity ratio between the crystalline (Pake function) and the intermediate (Exponential function; E_1) phases increase during crystallization (Fig. 5).

According to the “free volume” theory, the change in volume/density of the amorphous part of the polymer is assumed to be a result of change in mobility [31]. We tend to believe that this reduction in mobility will reduce not only the free volume of the amorphous phase, but also its density, as compared to the melt.

Fig. 6 shows that the parameter m of the Weibullian (W) function Eq. (2) changes with crystallization time from approximately 2 (Gaussian) at the start of the crystallization process, to a value somewhat larger than 1 (Lorenzian) during the primary crystallization time-regime. The physical reason for deriving an n value different from 1 or 2 is somewhat controversial. One explanation, might be that T_2 is not characterized by a single spin–spin relaxation time

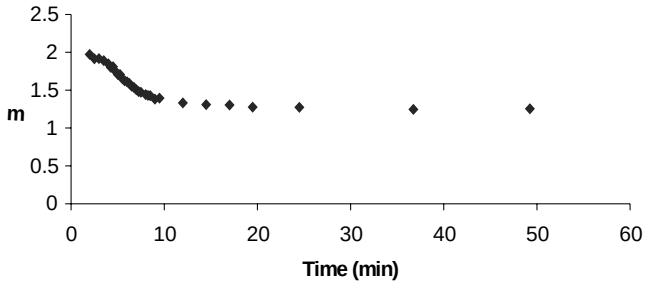

Fig. 6. Exponent n (Eq. (2)) vs. crystallization time.

but rather by a distribution of relaxation times, suggesting that a distribution of molecular mobility within the mobile phase exists.

4.3. Characterization of the crystalline/intermediate phases during the early stage of crystallization

As previously pointed out, the parameters α and β of the Pake function and the spin–spin relaxation rate ($1/T_{2,E_1}$) of the fast decaying Exponential function (E_1) of sample A cannot be reliably determined due to the small amount of crystalline/intermediate phases formed during the initial part of the crystallization process. However, performing the same type of NMR experiments on sample B it was possible to fit the "PWEE" model without introducing any

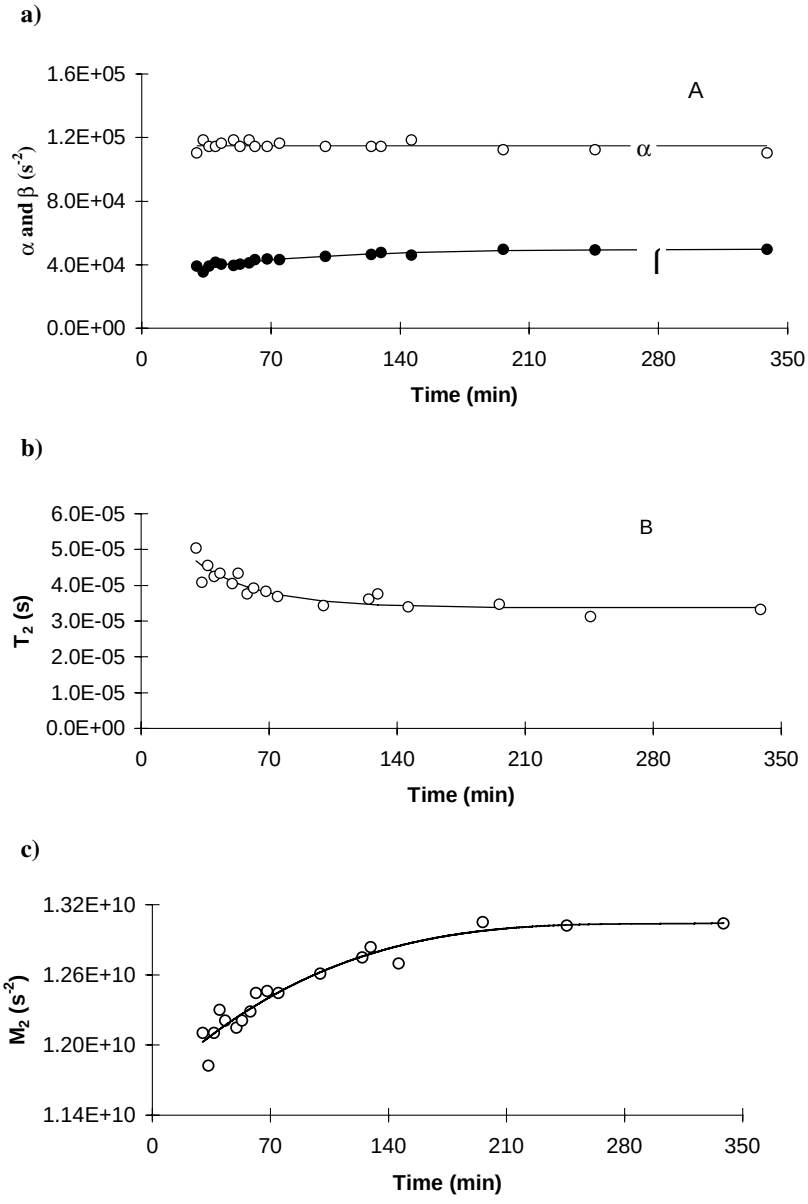

Fig. 7. Time dependence of the fitting parameters in the "FID-analysis" method obtained for sample A at 400 K. (a) ○ α; ● β from the crystalline part of the FID vs. time. (b) T_2 for component E_1, describing the intermediate part of the FID vs time. (c) Second moment (M_2) for the crystalline part of the FID vs time.

model constraints on α, β and T_{2,E_1}. Fig. 7a and b shows how the α and β parameters of the "Pake"-function and the spin–spin relaxation (T_{2,E_1}) of the Exponential function change during crystallization. The solid curves are calculated by simple exponential fits and have no theoretical significance. As can be seen, only the latter two parameters (β and T_{2,E_1}) change significantly with time and approach the limiting values ($t = \infty$) of $5 \times 10^4\ s^{-1}$ (β) and 33 μs (T_{2,E_1}), respectively. These values are — within experimental error — of the same order of magnitude as reported in previous work [13]. The parameter α is approximately constant ($1.15 \times 10^5\ s^{-1}$) and independent of time and equals the α-value determined for PE in previous work [13,14]. This suggests that the inter-nuclear distance, joining two protons on the same methylene carbon, does not change with crystallization time.

From the derived α and β values, the second moment, M_2, of the Pake function can be estimated according to Eq. (6) [21]:

$$M_2 = \frac{4}{5}\alpha^2 + \beta^2 \tag{6}$$

A plot of the second moment as a function of crystallization time is depicted in Fig. 7c (α was kept constant and equal to $1.15 \times 10^5\ s^{-1}$) and suggests that the molecular motion within the crystalline phase decreases slightly with crystallization time. The motional correlation time τ is estimated from Eq. (7):

$$\tau = \frac{\lambda}{\sqrt{M_2}} \tan\left[\frac{\pi}{2}\frac{M_2}{M_2^0}\right] \tag{7}$$

where $M_2^0 (= 2.28 \times 10^{10}\ s^{-2})$ is the limiting, rigid-lattice second moment [13]. Eq. (7) is derived from the Bloembergen, Purcell and Pound theory [32] with $\lambda = \sqrt{8 \ln 2}$ [33]. Applying Eq. (7) shows that the molecular correlation time increases with crystallization time from 22.3 μs to approximately 26.3 μs, i.e. an increase of approximately 18%. It must be emphasized that the molecular motional process within the crystalline phase is solely determined by the inter-molecular interaction, since only the β term Eq. (1) varies with time.

A similar analysis can be performed on the intermediate phase by replacing $\sqrt{M_2}$ by $1/T_2$ in Eq. (7) [13]. This approach shows that the correlation time of the intermediate phase increases with crystallization time from 5.9 μs to approximately 6.3 μs, and represents a slight decrease in the molecular motional freedom of approximately 6%. Note that the molecular motion within the intermediate phase is approximately four times faster than within the crystalline phase.

The crystalline and intermediate phases observed during the crystallization (Fig. 5) and the mobility of the two phases has to our knowledge not been reported by others. Terrill et al. [49] observed, however, that SAXS and WAXS measurements gave different onset of crystallization. In SAXS measurements some degree of order was observed before the method showed scattering. This was explained by phase separation of an ordered interchain and a random conformation before crystallization. This X-ray observation was the background for the developments of the spinodal crystallization theory [49–51].

4.4. Crystallization rate as a function of temperature

Fig. 8 shows how the signal intensity of the crystalline phase (P) changes with time during isothermal crystallization of the initially molten sample (sample A) at temperatures 391, 392, 393, 393.5, 394, 394.5 and 395 K (from left to right). Analogous isothermal crystallization curves have been obtained from density measurements and reveal — qualitatively — the same patterns as shown in Fig. 8 [2,34,35]. To gain more information on the isothermal crystallization process, the generalized Avrami model (Eq. (3a–c)) was adopted and fitted to the data in Fig. 8. The results of this analysis are summarized in Fig. 9, showing the temperature dependence of: (A) the Avrami exponent (β); (B) the time at which the secondary crystallization is initiated (t_d); and (C) the Avrami rate constant (k). The slight decrease in β with increasing crystallization temperature (Fig. 9(a)) suggests that the morphology changes somewhat with crystallization temperature. For instance, it is generally believed that formation of spherulite and disk shapes are characterized by a value of β equal to 3 and 2, respectively. A change in β with temperature has been reported by others [2,34,35].

The finding of β factors different from integer numbers is somewhat controversial since it is inconsistent with the originally derived Avrami model [25,26]. However, experiments resulting in β values different from integer (and half integer) have been reported [36–39].

The increase of t_d with decreasing crystallization temperature (Fig. 9(b)) suggests that the secondary crystallization process starts at a later time with increasing super-cooling. As shown in Fig. 5 the signal intensity ratio between the crystalline (Pake function) and the intermediate (Exponential function; E_1) phases increase during the primary crystallization (prior to t_d). It is not known whether this is due to a change in the thickness of the lamella formed or a thickening process.

The expected increase in crystallization rate with increasing super-cooling is clearly illustrated in Fig. 9(c), which shows the dependence of the Avrami crystallization rate (k) on crystallization temperature of the initially molten PE sample.

According to general crystallization theory [40], the rate of crystallization is determined by a competition between crystal growth rate and molecular transport rate. From thermodynamic arguments Eq. (8a) can be derived and shows how the (linear) growth rate (G) depends on crystallization

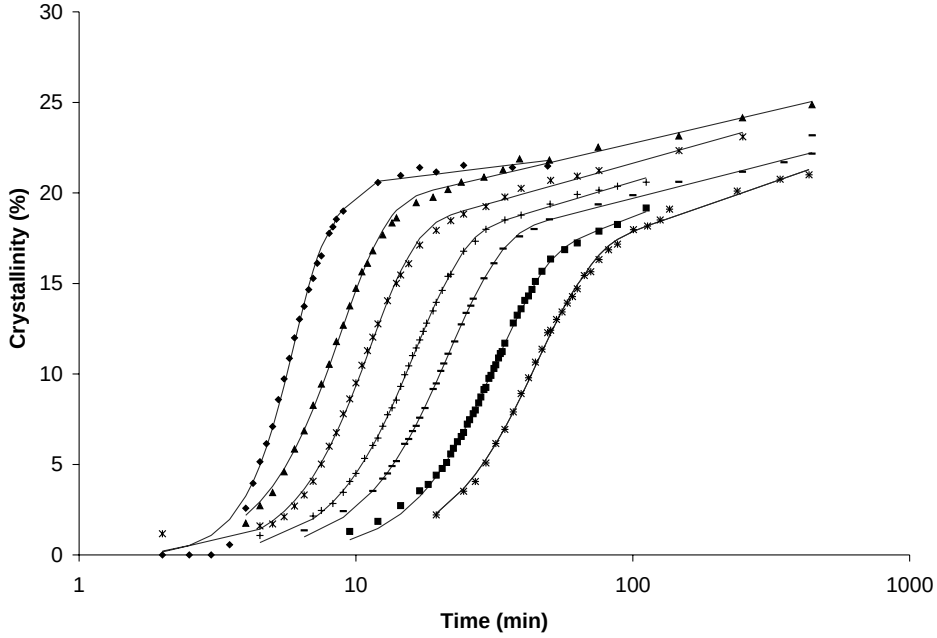

Fig. 8. Signal intensity of the pseudo-crystalline phase ($P + E_1$) as a function of time during isothermal crystallization of melted PE at temperatures 391, 392, 393, 393.5, 394, 394.5 and 395 K (from left to right).

temperature (T).

$$G = G_0 \exp\left[-\frac{U^*}{\mathrm{R}(T - T_\infty)}\right] \exp\left[-\frac{K_g}{T\Delta T f}\right] \tag{8a}$$

U^* is the activation energy for molecular transport in the vicinity of a growth front, R is the gas constant, T_∞ is the temperature where relevant molecular transport becomes ineffective, $\Delta T (= T_m^0 - T)$ represents the super-cooling, and T_m^0 is the equilibrium melting temperature. The parameter f is a correction factor, which compensates for the temperature change of the heat of fusion. K_g is a rather complex parameter involving the layer thickness of the crystallizing lamella, the crystallization enthalpy, the surface free energy of the fold surface and the free energy of the side surfaces [40,41]. Generally, K_g is expected to depend on the actual isothermal crystallization temperature [40].

To our knowledge, no theoretical or empirical relation between the Avrami rate constant (k) and the linear growth rate (G) has been reported. However, it seems — in particular cases — intuitively reasonable to expect the Avrami rate constant to depend on crystallization temperature in an analogous manner as described by Eq. (8a), i.e. by assuming G to be proportional to k:

$$G = \lambda k \tag{8b}$$

where λ is a constant.

Inserting $U^* = 6.3$ kJ/mole [42] and $T_\infty = 160$ K [43], the first exponential term in Eq. (8a) ($\exp\lfloor - U^*/\mathrm{R}(T - T_\infty)\rfloor$) changes with less than 6% within the temperature region investigated in this work. Hence, this term can be considered constant and independent of temperature. The melting temperature of sample A, T_m^0, can be estimated from Eq. (9) [44]:

$$\frac{1}{T_{m,ub}^0} - \frac{1}{T_m^0} = \frac{\mathrm{R}}{\Delta H_u} \ln(X_A) \tag{9}$$

in which $T_{m,ub}^0$ (= 418.5 K) [45] and ΔH_u (= 3970 J/mol) [46] are the melting temperature and the heat of melting of an unbranched PE, respectively. X_A is the co-monomer content. T_m^0 was calculated to be 415.3 and 418.2 K for sample A and sample B, respectively. The factor f, which can be approximated by the expression $f \approx 2T/(T + T_m^0))$ [41], varies by less than 1% within the crystallization temperatures region reported in this work and can be set equal to one. Combining Eq. (8a and b) gives the following simple expression for the temperature dependence of the Avrami rate constant k:

$$k = k_0 \exp\left[-\frac{K_g}{T\Delta T}\right] \tag{10}$$

where k_0 is a constant. The solid curve in Fig. 9(c) represents non-linear least squares fit to Eq. (10) with $K_g = 1.33 \times 10^5$ K2. This is more than 25% less than the theoretical value of K_g ($= 1.8 \times 10^5$ K^2), as calculated by Hofmann [47]. For sample B a $K_g = 1.79 \times 10^5$ K^2 (95% confidence interval; 1.44×10^5–2.15×10^5 K^2) was determined and is in excellent agreement with the theoretical value. Keeping in mind that the uncertainty in the derived rate constants (k) is less than 3% and that the uncertainty in temperature is approximately 0.5 K, the model fit in Fig. 9(c) is rather poor. However, dividing the temperature interval into two regions, Eq. (10) can be fitted to each region as

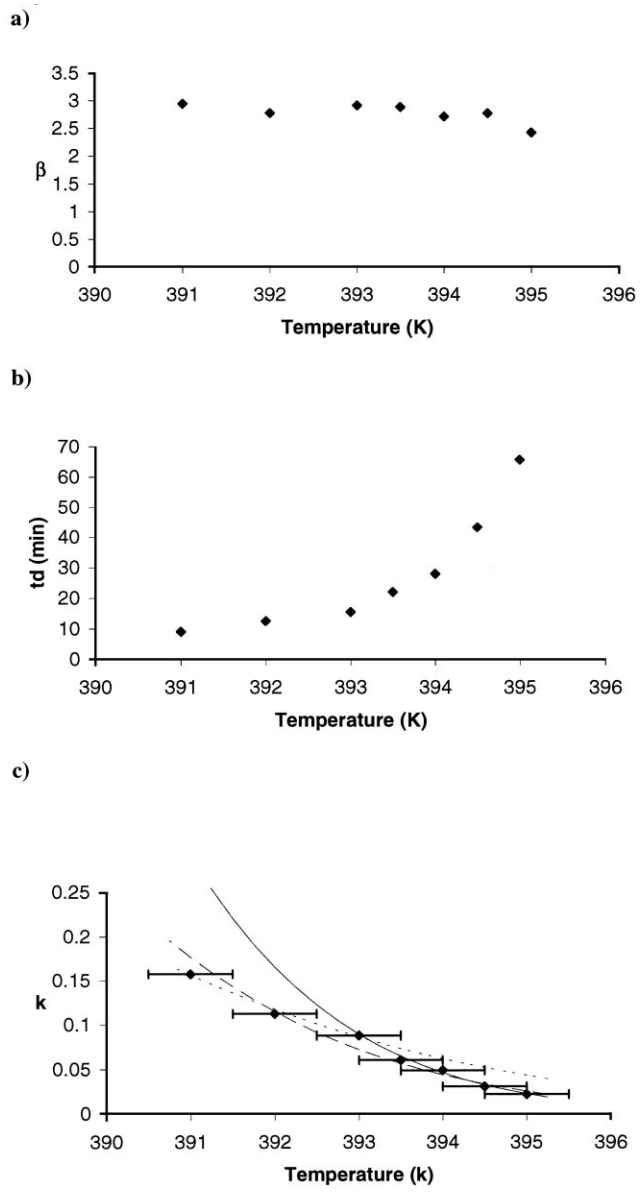

Fig. 9. Fitting of Eq. (3c) to the pseudo-crystalline phase ($P + E_1$) and the amorphous phase ($W + E_2$). (a) Shows the Avrami exponent (β) as a function of temperature. (b) Onset of the secondary crystallization (t_d) with temperature. (c) Avrami crystallization rate (k) as a function of temperature. ○ Measured k values; — — fit of Eq. (8) to all the data points; — fit to the high-temperature region; – – – – fit to the low-temperature region.

shown by the dotted curves in Fig. 9(c) and results in a significantly better fit. The corresponding K_g value was determined to be $1.74 \times 10^5\ K^2$ (95% confidence interval; $1.46.10^5$–$2.01 \times 10^5\ K^2$) and $0.85 \times 10^5\ K^2$ (95% confidence interval; 0.41×10^5–$2.11 \times 10^5\ K^2$), respectively. Such a change in K_g within different temperature regions has been reported elsewhere. For instance, Lambert and Phillips [41,48] have reported on a change in K_g for PE at approximately the same temperature as observed in this work. The temperature at which K_g changes has been claimed to depend on both molecular weight [48] and on the content of chain-branching [41,48].

Considering the limited number of data points and the inherent assumptions made in deriving Eq. (10), one should be careful in putting to much weight on the derived K_g values. Also, the assumption of a linear relation between the Avrami rate constant k and G (Eq. (8b)) may be questionable and needs further experimental and theoretical support. Additional experimental data on PE samples with different degree of branching and molecular weights are necessary to justify Eq. (10).

4.5. Requirements for probing crystallization by the "FID-analysis" technique

Temperature regulation control, heat transfer and inherent spin–lattice relaxation times of the different phases of PE are crucial and decisive parameters when attempting to probe isothermal crystallization by the present NMR technique.

A number of relaxation time measurements (T_1 and T_2) on melted and semi-crystalline PE has been reported in the literature [15,17], suggesting that the spin–lattice relaxation time is of the order of one second. Hence, a quantitative sampling of a FID signal (1 scan) can be obtained within approximately 5 s. If the number of measurements required to obtain a reliable crystallization curve (signal intensity vs crystallization time) is set to 20, a minimum experimental time of 100 s is obtained.

Also, the crystalline growth rate and crystalline morphology may affect the temperature region amenable for NMR measurements. From K_g and β obtained in this work, a region of super-cooling amenable for NMR measurements can be estimated to be approximately 30 K. Using the same approach as just outlined and assuming the upper time limit to be 12 h (primary crystallization should not take more than 12 h), an estimated temperature region of super-cooling of approximately 9.3 K can be estimated. Thus — in practice — the present NMR technique will enable isothermal crystallization studies to be performed within a super cooling range of approximately 10 K.

Acknowledgements

We are grateful to Borealis AS for making the PE samples available for NMR characterization and for financial support.

Appendix A

Assuming the time dependence of the NMR signal intensity (I) of molten (M) and amorphous (A) phases to be described by an Avrami type of equation (Eq. (3a)) during isothermal crystallization within the primary crystallization time regime, we can write:

$$I_X(t) = I_{X\infty} - (I_{X\infty} - I_{X0}) \exp(-[k_X t]^{\beta_X}) \quad \text{(A1)}$$

where X = M and A. The other symbols are defined previously (see Eq. (3a)). Since the mobile phase, represented by (A + M), is completely molten at the start ($t = 0$) of the crystallization we can write $M = M_0$ and $A = 0$. Assuming the same mobile phase to be completely amorphous at the end ($t = \infty$) of the crystallization process we can set $A = A_\infty$, and $M = 0$, hence:

$$I_A(t) = I_{A\infty}[1 - \exp\lfloor -\lfloor k_A t)^{\beta_A}\rfloor\rfloor \tag{A2}$$

$$I_M(t) = I_{M_0}\exp\lfloor -(k_M t)^{\beta_M}\rfloor \tag{A3}$$

We have previously noted that the overall mobile phase can be well approximated by a single Avrami equation of the form:

$$I = A_\infty - (A_\infty - M_0)\exp(-[kt]^\beta) \tag{A4}$$

where

$$I = I_A + I_M \tag{A5}$$

Inserting Eqs. (A2)–(A4) into Eq. (A5) gives $\beta_A = \beta_M = \beta$ and $k_A = k_M = k$. Hence f in Eq. (5b) can be written:

$$f = \frac{A}{A+M} = \frac{I_{A\infty}(1 - \exp[-(kt)^\beta])}{I_{M_0}\exp[-(kt)^\beta] + I_{A\infty}(1 - \exp[-(kt)^\beta])}$$

$$= \frac{\theta_{A\infty}(1 - \exp[-(kt)^\beta])}{\theta_{A\infty} + (1 - \theta_{A\infty})\exp[-(kt)^\beta]} \tag{A6}$$

where $\theta_{A\infty} = I_{A\infty}/I_{M0}$. Inserting Eq. (A6) into Eq. (5b) and rearranging gives Eq. (5c).

References

[1] Mandelkern L. In: Dosier M, editor. Crystallization of polymers. 1993. p. 25–37.
[2] Ergoz E, Fatou JG, Mandelkern L. Macromolecules 1972;5:147–57.
[3] Kitamaru R, Horii F. Adv Polym Sci 1978;26:137–78.
[4] Kitamaru R, Horii F, Murayama K. Macromolecules 1986;19:636–43.
[5] Chen J, Fone M, Reddy VN, Schwartz KB, Fisher PH, Wunderlich B. J Polym Sci, Part B: Polym Phys 1994;32:2683–93.
[6] Kitamaru R, Horii F, Zhu Q, Basset DC, Olley RH. Polymer 1994;35:1171–81.
[7] Boyd RH. Polymer 1985:323–447.
[8] Rybnikar F. J Polym Sci 1960;44:517–22.
[9] Buckser S, Tung LH. J Phys Chem 1959;63:763–5.
[10] Banks W, Gordon M, Roe R-J, Sharples A. Polymer 1963;4:61–74.
[11] Chen J, Fone M, Reddy VN, Schwartz KB, Fisher PH, Wunderlich B. J Polym Sci, Part B: Polym Phys 1994;32:2683–93.
[12] Kitamaru R, Horii F. Adv Polym Sci 1978;26:137–78.
[13] Kristiansen PE, Hansen EW, Pedersen B. Polymer 1999;41:311.
[14] Kristiansen PE, Hansen EW, Pedersen B. J Phys Chem 1999;103:3552.
[15] Jurkiewicz A, Tritt-Goc J, Pislewski N, Kunert KA. Polymer 1985;26:557.
[16] Brereton MG, Ward IM, Boden N, Wright P. Macromolecules 1991;24:2068.
[17] Ueda T, Takeda S, Nakamura N, Chihara H. Bull Chem Soc Jpn 1991;64:1299.
[18] Hansen EW, Kristiansen PE, Pedersen B. J Phys Chem 1998;102:5444.
[19] Pake GE. J Chem Phys 1948;16:327.
[20] Engelsberg M, Lowe IJ. Phys Rev 1974;10:822.
[21] Look DC, Lowe IJ, Nortby JA. J Chem Phys 1966;44:3441.
[22] Abramowitz SI. Handbook of mathematical functions. New York: Dover, 1970 (p. 300–3).
[23] Brereton MG. J Chem Phys 1991;94:2068.
[24] Dadayli D, Harris RK, Kenwright AM, Say BJ, Sunnetcioglu MM. Polymer 1995;35:4083.
[25] Avrami M. J Chem Phys 1939;7:1103.
[26] Avrami M. J Chem Phys 1940;8:812.
[27] Schultz J. Polymer materials science. Englewood Cliffs, NJ: Prentice-Hall, 1974 (p. 380–417).
[28] Eamor MW, Shamg NY. Polym Engng Sci 1998;39:583.
[29] Kovacs AJ. International Symposium on Macromolecular Chemistry, Milano, 1954. Rierca Sci 1955;25A:668.
[30] Bremner T, Rudin A. J Polym Sci, Polym Phys 1992;30:1247.
[31] Cowie JMG. Polymer chemistry and physics of modern materials. 2nd ed. London: Blackie, 1991.
[32] Bloemberger N, Purcell EM, Pound RV. Phys Rev 1948;73:679.
[33] Kubo R, Tomita KJ. J Phys Soc Jpn 1954;9:888.
[34] Keith HD, Padden FJ. J Appl Phys 1964;35:1286.
[35] Okada T, Saito H, Inoue T. Polymer 1994;35:5699.
[36] Holland VF, Lindenmeyer PH. J Polym Sci 1962;57:589.
[37] Price FP, Kilb RW. J Polym Sci 1962;57:589.
[38] Barnes WJ, Luetzel WG, Price FP. J Phys Chem 1961;65:1742.
[39] Cheng SZD, Wunderlich B. Macromolecules 1988;21:3327.
[40] Hofmann JD, Davis GT, Lauritzen Jr JI. In: Hannay NB, editor. Treatise on solid state chemistry, vol 3. New York: Plenum Press, 1976 (chap. 7).
[41] Lambert WS, Phillips PJ. Macromolecules 1994;27:3537.
[42] Suzuki T, Kovacs AJJ. Polym J 1970;1:82.
[43] Boyd RH. Macromolecules 1984;17:903.
[44] Flory PJ. J Chem Phys 1949;17:223.
[45] Flory PJ, Vrij A. J Am Chem Soc 1963;85:3548.
[46] Mandelkern L. Rubber Chem Technol 1959;32:1392 (see p. 1403).
[47] Hofmann JD. Polymer 1983;24:3.
[48] Lambert WS, Phillips PJ. Polymer 1996;37:3585.
[49] Ryan AJ, Fairclough JPA, Terrill NJ, Olmsted PD, Poon WCK. Faraday Discuss 1999;112:13.
[50] Olmsted PD, Poon WcK, McLeish TCB, Terrill NJ, Ryan AJ. Phys Rev Lett 1998;81:373.
[51] Terrill NJ, Fairclough PA, TownsAndrews E, Komanschek BU, Young RJ, Ryan AJ. Polymer 1998;11:2381.